# Enhanced Cu₂S/CdS Coaxial Nanowire Solar Cells by Piezo-Phototronic Effect

Caofeng Pan, Simiao Niu, Yong Ding, Lin Dong, Ruomeng Yu, Ying Liu, Guang Zhu, and Zhong Lin Wang*

School of Materials Science and Engineering, Georgia Institute of Technology, Atlanta, Georgia 30332-0245, United States

**S** Supporting Information

**ABSTRACT:** Nanowire solar cells are promising candidates for powering nanosystems and flexible electronics. The strain in the nanowires, introduced during growth, device fabrication and/or application, is an important issue for piezoelectric semiconductor (like CdS, ZnO, and CdTe) based photovoltaic. In this work, we demonstrate the first largely enhanced performance of n-CdS/p-Cu₂S coaxial nanowire photovoltaic (PV) devices using the piezo-photo-tronics effect when the PV device is subjected to an external strain. Piezo-phototronics effect could control the electron—hole pair generation, transport, separation, and/or recombination, thus enhanced the performance of the PV devices by as high as 70%. This effect offers a new concept for improving solar energy conversation efficiency by designing the orientation of the nanowires and the strain to be purposely introduced in the packaging of the solar cells. This study shed light on the enhanced flexible solar cells for applications in self-powered technology, environmental monitoring, and even defensive technology.



**KEYWORDS:** Cu₂S/CdS coaxial nanowire, nanowire PV devices, piezo-phototronics effect, enhanced energy conversion efficiency
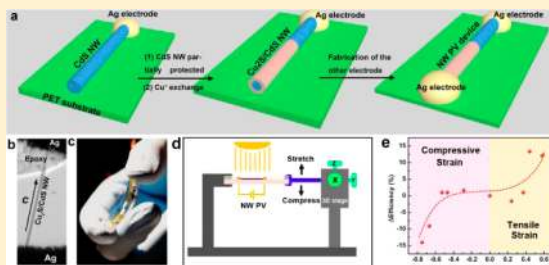
Searching for renewable and green energy is one of the most urgent challenges to the sustainable development of human civilization owing to the threat of global warming and energy crises. Solar is probably the most abundant clean and renewable energy. Semiconductor nanowires (NWs) have a lot of advantages as candidates for photovoltaic (PV) applications[1−3] due to their large surface-to-volume ratio, better charge collection,[4] and the possibility of enhanced absorption through light trapping;[5,6] at the other side, nanowires will cause large surface and interface recombination, which could be overcome by surface passivation[7] and epitaxial growth of p−n junctions.[8] NWs-based PV has great application in flexible power source compared to bulk materials. In such case, the strain in the NWs, introduced during growth, device fabrication, and/or application, is an important issue for piezoelectric semiconductor (like CdS, ZnO, and CdTe) based PVs. Although theoretical study has predicted piezoelectric effect on NW PV,[9] experimental verification is still unavailable. Here, we report the enhanced performance of the piezoelectric n-CdS/p-Cu₂S core−shell NW PV devices by a factor of 70% using the piezo-phototronic effect, which could control the electron−hole pair generation, transport, separation, and/or recombination at p−n junction via applied strain, thus tuning the performance of the PV devices. This effect offers a new concept for increasing solar energy conversion efficiency and has a bright future in the applications of flexible solar cell and self-powered technology.

NW photovoltaics (PV) have been the subject of research for enhancing the energy conversion efficiency and possibly reducing the material and fabrication costs. The core−shell geometry of NWs is proposed to be able to enhance the efficiency of charge collection by shortening the paths traveled by minority carriers,[7,8,10] increasing the optical quality of the material,[11,12] or strain engineering of the bandgap.[11] However, the strain in the NW is a critical issue for such core−shell NW PV devices. First, for decreasing electron−hole interface recombination and increasing charge collection efficiency, a single crystal epitaxial p−n structure is highly desirable, but these epitaxial hetrojunction NWs introduce static strain as a result of a misfit between the inherent crystal lattices between the core and shell materials. Second, flexible PV devices have been the subject of research for powering flexible electronics and devices,[13,14] which inevitably introduce strain during the operation. Thus, our goal here is to study the piezo-phototronic effect on the performance of piezoelectric PV devices made using single crystal epitaxial coaxial structures.

Our PV device is based on epitaxial coaxial NWs with p-Cu₂S as shell and n-CdS as core. CdS is a piezoelectric material with wurzite structure that has noncentral symmetry. Because of the polarization of ions in CdS NW, a piezopotential is created by applying a stress. Owing to the simultaneous possession of piezoelectricity and semiconductor properties, the piezopotential created in the core has a strong effect on the carrier transport at the interface/junction, known as piezo-phototronic effect, which is to use the piezopotential created in the wurzite
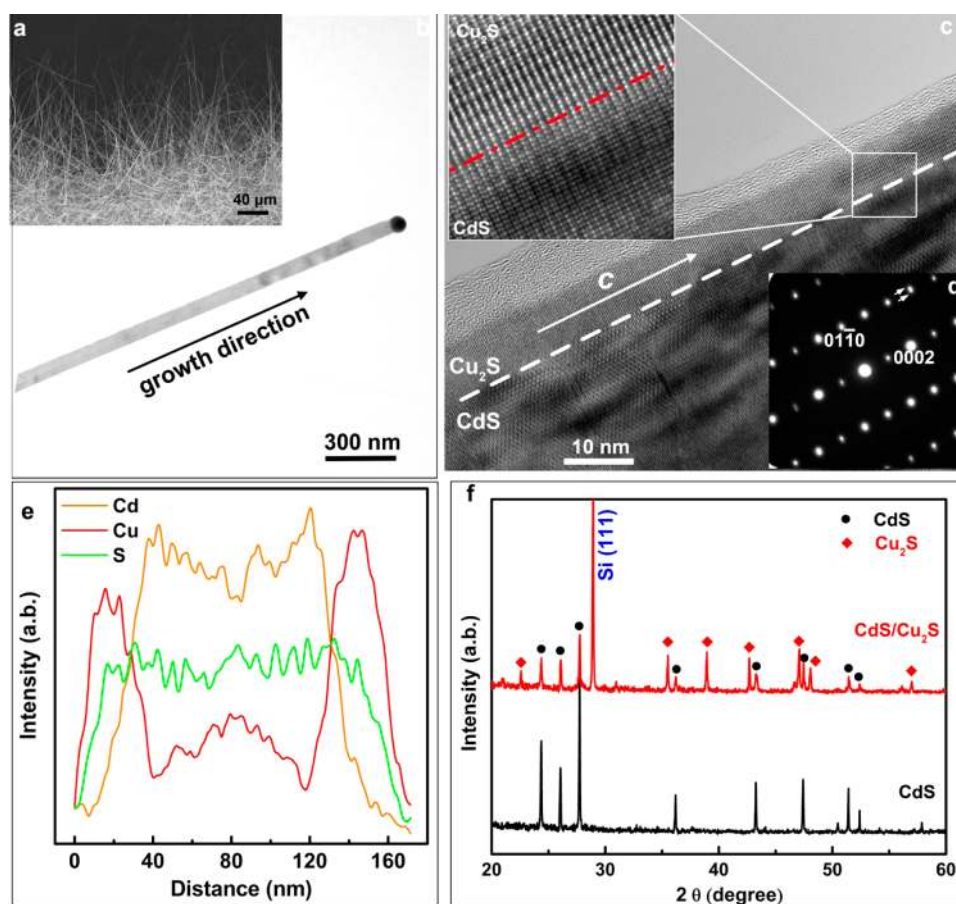
**Figure 1.** Synthesis and characterization of the coaxial $Cu_2S/CdS$ NWs. (a) SEM image of the morphology of the as-synthesized CdS NWs. (b) A low-magnification TEM image of an individual as-fabricated CdS NW, which is proved to be synthesized via a VLS method by the remaining gold catalyst on the tip of the NW. (c,d) Representative high-resolution TEM image and electron diffraction pattern of the $Cu^+$ treated $Cu_2S/CdS$ coaxial NWs. The dashed line indicates the interface between CdS and $Cu_2S$. The enlarged image clearly shows high-quality epitaxial crystalline at the interface of the coaxial NWs. (e) Line scan chemical profile across the NW acquired using the energy-dispersive X-ray spectroscopy (EDS). (f) X-ray diffraction spectra of CdS (the black trace) and $Cu_2S/CdS$ coaxial NWs (the red trace). The peaks in the red trace marked with black dots belong to CdS core, and the peaks marked with red dots belong to $Cu_2S$ shell.
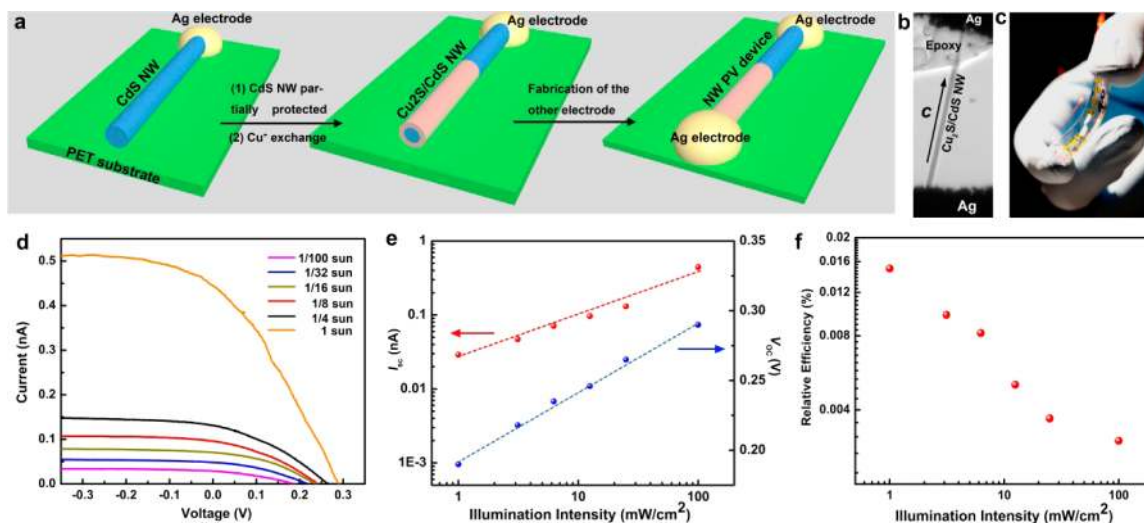


**Figure 2.** Fabrication and characterization of $CdS-Cu_2S$ core–shell nanowire PV devices. (a) Schematic of the fabrication process. From left to right, a CdS (blue) NW with metal contact at one end is partially immersed into CuCl solution to form a layer of $Cu_2S$ (pink) shell, and then metal contact at the other end was fabricated on the $Cu_2S$ shell. The polymer masking step is not shown. (b,c) Optical microscopy and digital image of a typical PV device. (d) $I-V$ characteristic of a core–shell nanowire PV device under an illumination from 1% sun to a full sun (AM 1.5). (e) Light intensity dependence of the photocurrent ($I_{SC}$) and open-circuit voltage ($V_{OC}$). (f) Light intensity dependence of the conversion efficiency ($\eta$).
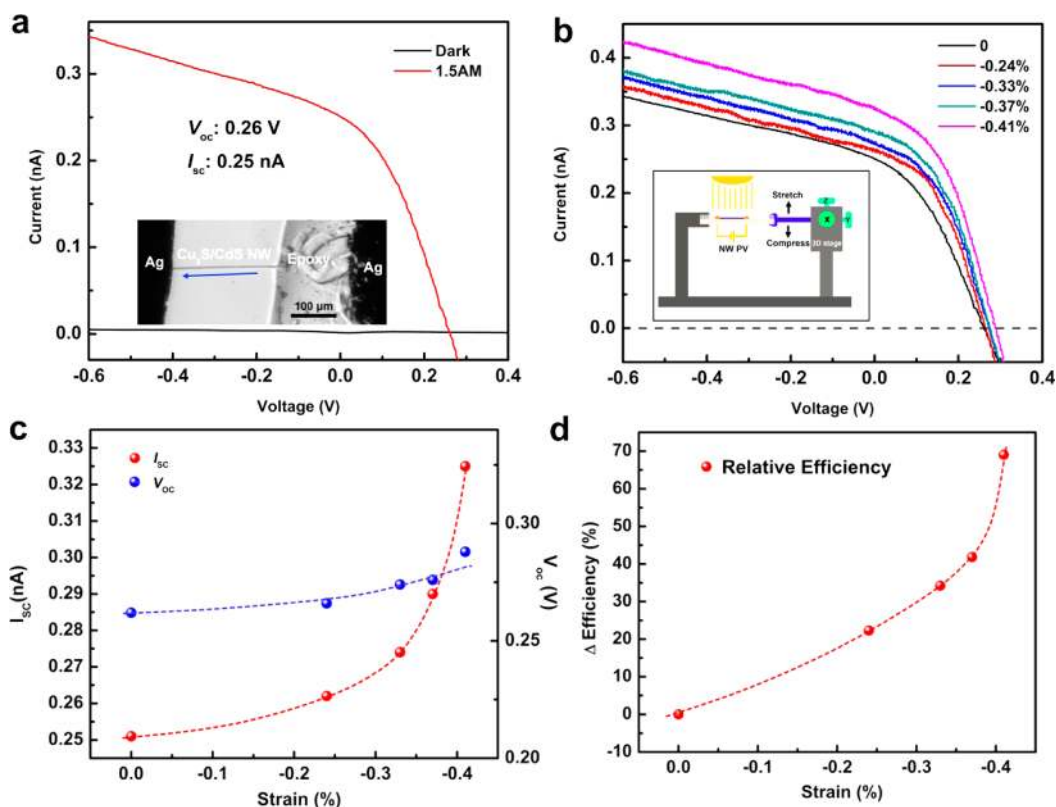
**Figure 3.** The performance of the $Cu_2S$/CdS coaxial NW solar cell under compressive strains. (a) The dark and 1.5AM illuminated $I-V$ curve of the NW solar cell. The short circuit current is 0.25 nA, and the open circuit voltage is 0.26 V without applied strain. The insert is an optical microscopy image of the $Cu_2S$/CdS coaxial NW solar cell. (b) The $I-V$ curve of the same NW solar cell under different compressive strain, clearly indicating the current increase with increasing external compressive strain. The schematic of the measurement setup for studying the piezo-phototronic effect PV devices is demonstrated as inset. (c,d) Dependence of the open circuit voltage (c), the short circuit current (c), and relative efficiency change (d) on the strain. The data plotted in panels c and d are extracted from panel b.

structure crystal to control the carrier generation, transport, separation, and/or recombination for improving the performance of optoelectronic devices. It is demonstrated that the piezo-phototronic effect can greatly improve the sensitivity of photon detectors,[15] enhance the light emission intensity and LED efficiency,[16] and improve the photoelectrochemical efficiency.[17] Here, we tune the performance of the n-CdS/p-$Cu_2S$ coaxial NW PV devices by the piezo-phototronic effect when the devices are subjected to strain, which offers a new concept for improving solar energy conversation efficiency.

The n-CdS NW is synthesized via a vapor–liquid–solid (VLS) method,[18] which gives high quality and long NWs. The morphology of the as-fabricated CdS NWs is presented in Figure 1a, with lengths of several hundreds of micrometers and diameters varying from tens of nanometers to several micrometers. Figure 1b is a low-magnification transmission electron microscopy (TEM) image of an individual as-fabricated n-CdS NW, showing a uniform shape of the NW. The epitaxial shell layer is obtained using a solution-based cation exchange reaction[19−23] that creates a heterojunction between the single-crystalline CdS core and single-crystalline $Cu_2S$ shell. A high-resolution TEM (HRTEM) image and the selected area diffraction (SAD) pattern of a CdS/$Cu_2S$ coaxial NW are presented in Figure 1c,d, respectively. It indicates that the growth direction of the coaxial NW is [0001] (c-axis), and the thickness of the shell layer is 10−15 nm. The enlarged image clearly shows high-quality epitaxial crystallinity at interface of the coaxial NWs. Figure 1e is an in situ energy-

dispersive X-ray (EDX) line scan across the entire NW, which clearly shows that the Cu located at the shell, while the Cd located at the core. Both the Moiré fringes in the HRTEM image, the splitting of the diffraction spots (marked by the white arrows in Figure 1d) and the EDX line scale profile confirm the core/shell heteroepitaxial junction between the CdS core and $Cu_2S$ shell.

The fabrication process of the coaxial CdS/$Cu_2S$ NW PV devices is demonstrated in Figure 2a. First, we carefully chose a long CdS NW and dispersed it onto a polyethylene terephthalate (PET)/or a polystyrene (PS) substrate; one end of the CdS NW was fixed by silver paste, serving as an electrode. After that a layer of epoxy was used to cover the silver-fixed side of the CdS, preventing $Cu^+$ from exchange in the following steps. Cation conversion was performed by dipping the CdS NW into CuCl solution at 50 °C for 10 s. It was then thoroughly rinsed with deionized water, ethanol, and isopropanol (IPA) and blown dry with nitrogen. Subsequently, the other end of the coaxial NW was also fixed with silver paste, contacting with the p-$Cu_2S$ layer. An oxygen plasma was carried out for improving the contact between CdS/Ag and $Cu_2S$/Ag before each step. Finally, the entire fabricated device is packaged with polydimethylsiloxane (PDMS), preventing the device from contamination and damage. An optical microscope image of an as-fabricated device is shown in Figure 2b.

The solar cell is irradiated using a solar simulator (300 W Model 91160, Newport) with an AM 1.5 spectrum distribution calibrated against a NREL reference cell to accurately simulate
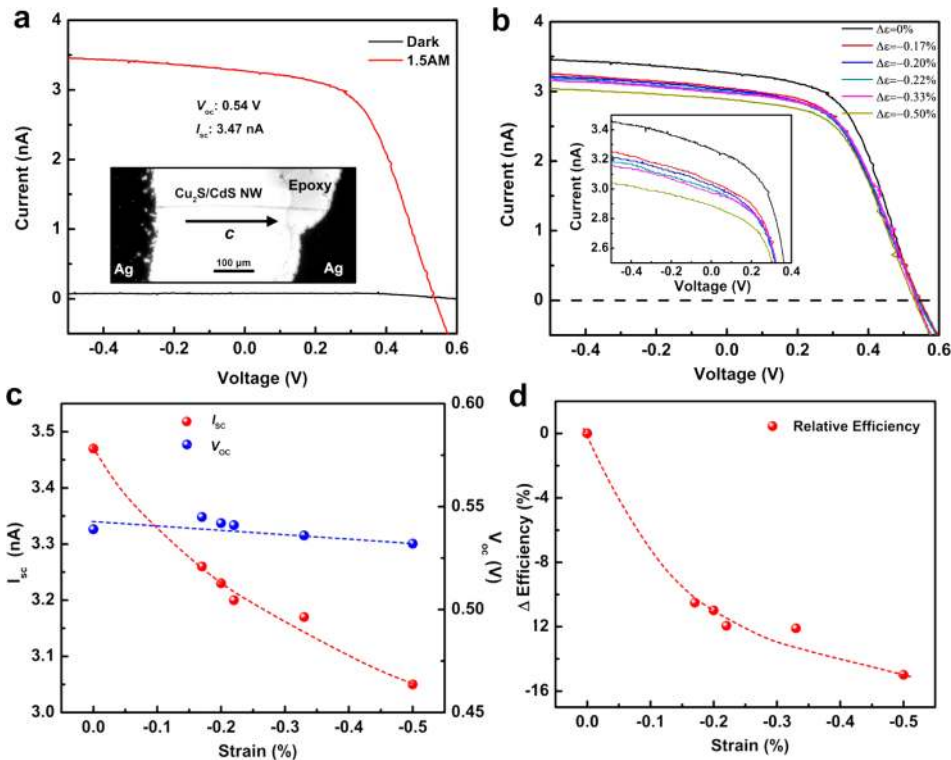
**Figure 4.** The performance of the $Cu_2S/CdS$ coaxial NW solar cell under compressive strains. (a) The dark and 1.5AM illuminated $I-V$ curve of the NW solar cell. The short circuit current is about 3.47 nA, and the open circuit voltage is 0.54 V without applied strain. The inset is an optical microscopy image of the $Cu_2S/CdS$ coaxial NW solar cell. (b) The $I-V$ curve of the same NW solar cell under different compressive strain. The insert is an enlarged plot of the $I-V$ curve, clearly indicating the current decrease with increasing external compressive strain. (c,d) Dependence of the open circuit voltage (c), the short circuit current (c), and relative efficiency change (d) on the strain. The data plotted in panels c and d are extracted from panel b.

full-sun intensity (100 mW/cm$^2$). The as-measured $I-V$ characteristic of the coaxial NW PV devices under different illumination intensities is presented in Figure 2c. This nanowire PV devices were 225 $\mu$m long and 5.8 $\mu$m in diameter and yielded a short-circuit current $I_{SC}$ of 0.44 nA under a full-sun intensity. The performance of the PV device dropped with the illumination intensity decreasing from a full sun to 1% of a sun: the short-circuit current $I_{SC}$ dropped from 0.44 to 0.03 nA, while the open-circuit voltage ($V_{OC}$) dropped from 0.29 to 0.19 V, with a rate ($\Delta V_{OC}/\Delta \ln(I_{illum}) = 50$ mV, where $I_{illum}$ is the relative illumination intensity) comparable to that of the silicon nanowire[2] ($\Delta V_{OC}/\Delta \ln(I_{illum}) = 56$ mV) and $Cu_2S$ thin film PVs[24] ($\Delta V_{OC}/\Delta \ln(I_{illum}) = 39$ mV). The corresponding relative conversion efficiency (conversion efficiency/illumination intensity) under different illumination intensities is plotted in Figure 2e. The higher relative convention efficiency under low illumination conditions implies that our PV devices may be suitable for some special working conditions, such as in indoor applications. The main reason is that the charge collection efficiency is higher for the PV devices under low light intensity. When the light intensity is low, the amount of the light generated electron−hole pairs is small, it can be sufficiently separated with low carrier recombination at the interface; but at a high light intensity, there are a large number of light generated electron−hole pairs, which cannot be sufficiently separated, and results in a high recombination at the interface. The performance of such coaxial $CdS/Cu_2S$ NW PV devices can be increased by optimizing the design, structure, doping, semiconductor/metal contacts, working condition and so on. Tang et al. reported a very high FF PV device with the output

performance of $V_{OC} = 0.61$ V, $I_{SC} = 147$pA, FF = 80.8%, and $\eta$ = 5.4%,[3] this will let such kind of PV devices have bright future in the practical application.

To investigate the piezo-phototronics effect on the PV devices, the PV devices were subjected to compressive strain, and the results are presented in Figure 3 and Figure 4. The schematic of the measurement setup for studying the piezo-phototronic effect PV devices is demonstrated as insert upper-right in Figure 3b. One end of the PS substrate was fixed tightly on a manipulation holder, with the other end free to be bent. A three-dimensional (3D) mechanical stage with movement resolution of 1 $\mu$m was used to apply the strain on the free end of the PS substrate, to introduce a compressive or tensile strain, which can be calculated according to Yang et al's work.[25]

Because of the asymmetric polarity of the CdS NW, there are two different configurations of our $CdS/Cu_2S$ NW PV devices when the $c$-axis of the CdS NW pointing upward: one is $Cu_2S$ shell only located at the upper part of the CdS NW, note as configuration I (Figure 5d); the other is $Cu_2S$ shell only located at the lower part of the CdS NW, note as configuration II (Figure 5g). The piezo-phototronic effect on a PV device with configuration I is illustrated in Figure 3; these nanowire PV devices were 220 $\mu$m long and 4.95 $\mu$m in diameter and yielded an $I_{SC}$ of 0.25 nA and a $V_{OC}$ of 0.26 V under a full-sun intensity (Figure 3a). The $I-V$ curves of the PV device subjected to strains were presented in Figure 3b. The performance of this PV device was enhanced when the PV device was subjected to a compressive strain up to −0.41%, and the $I_{SC}$ and the $V_{OC}$ under different strains were extracted and plotted in Figure 3c. It can be found that the $I_{SC}$ increased from 0.25 to 0.33 nA,
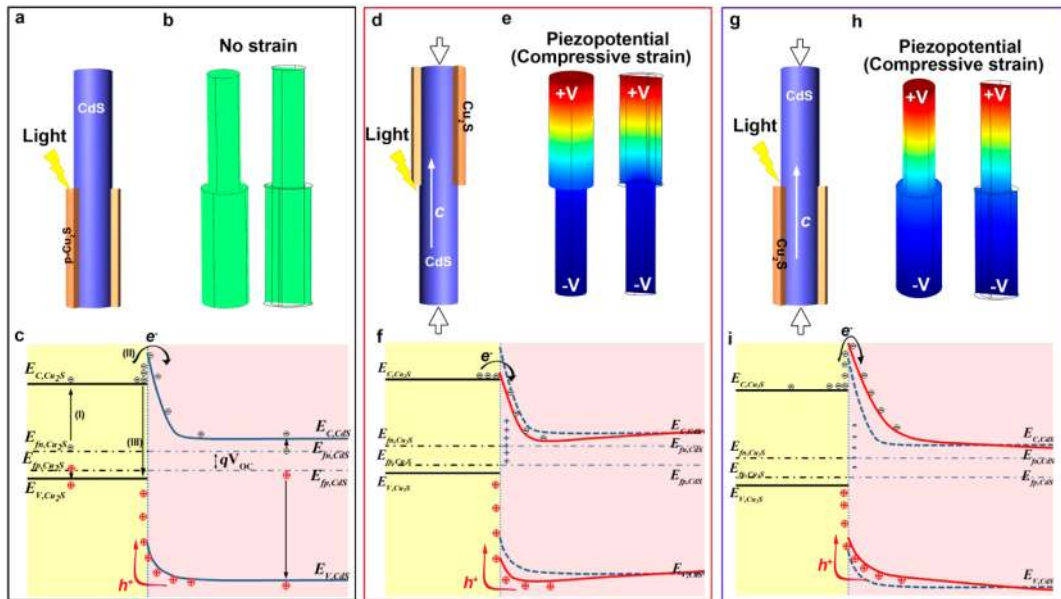
**Figure 5.** Schematics and energy band diagrams demonstrate the piezo-phototronic effect on coaxial piezoelectric nanowire solar cells. (a–c) Schematics (a), numerically calculated piezopotential distribution (b, both the tilt-view (left) and cross section-view (right)), and the corresponding energy band diagram (c) of a strain-free coaxial piezoelectric NW solar cell. (d–f) Schematics (d), numerically calculated piezopotential distribution (e), and the corresponding energy band diagram (f) of a coaxial piezoelectric NW solar cell under compressive strain for a PV device with configuration (I). The upper part of the CdS NW is positively charged, while the lower part is negatively charged due to the piezoelectric potential under compressive strain. The positive charges at CdS side lower the conduction and valence bands of CdS at the interface of the p−n junction, which decrease the barrier height at the interface of the heterojunction, resulting in an enhancement of the PV performance. (g–i) Schematics (g), numerically calculated piezopotential distribution (h), and the corresponding energy band diagram (i) of a coaxial piezoelectric NW solar cell under compressive strain for a PV device with configuration II. The negative charges at the CdS/Cu$_2$S interface lift up the conduction and valence band of CdS at the interface of the p−n junction, thus resulting in a drop of the PV device. The dashed line in (f) and (i) represents the original conduction and valence band of the piezopotential along the coaxial nanowires.

about 32% incensement, while the $V_{OC}$ varied between 0.26 and 0.29 V, about 10% fluctuation. As dominated by the enhancement of the output current, the relative convention efficiency change of this PV device increased about 70% when a −0.41% compressive strain was applied (Figure 3d).

The piezo-phototronics effect on another PV device with configuration II is illustrated in Figure 4, which is 328 μm long and 6.7 μm in diameter and yielded an $I_{SC}$ of 3.47 nA and a $V_{OC}$ of 0.54 V under a full-sun intensity (Figure 4a). Different from the previous one, the performance of this device dropped when the applied compressive strain was increased, as shown in Figure 4b. The $I_{SC}$ and the $V_{OC}$ under different strains were extracted and plotted in Figure 3c. It can be found that the $I_{SC}$ dropped from 3.47 to 3.05 nA for nearly 14%, while the $V_{OC}$ varied between 532 and 545 mV for only 2% fluctuation. As a result of the decreasing of the output current, the energy convention efficiency decreased about 15% when a 0.5% compressive strain was applied. By comparing the two NW PVs shown in Figures 3 and 4, we found that such piezo-phototronics effect has larger impact/enhancement on a PV of lower FF and lower efficiency. For example, the performance increases about 70% for the PV shown in Figure 3, which has a lower output performance, while the performance only changes 15% for the PV shown in Figure 4, which has a higher output performance. Such enhanced performance of the PV devices under a compressive strain is suggested arising from the effective decrease of the barrier height between Cu$_2$S and CdS at the hetrojunction interface[26] as a result of the band modification caused by piezoelectric polarization charges, as discussed in the follows.

A theoretical model is proposed to explain the piezo-phototronic effect on the performance of the PV devices using energy band diagrams, as shown in Figure 5. CdS has a noncentral symmetric wurzite structure in which the cations and anions are tetrahedrally coordinated. A straining on the basic unit results in a polarization of the cations and anions, which is the cause of the piezopotenital inside the crystal. For a coaxial n-CdS/p-Cu$_2$S NW PV device, schematic structure, numerically calculated piezopotential distribution, and the corresponding energy band diagram (with a barrier at the interface[26]) of a strain-free coaxial piezoelectric NW PV device are presented in Figure 5a−c, respectively. For a typical PV device, there are three key processes for dictating its performance as shown in Figure 5c: (I) generation rate of the electron−hole pairs under the illumination; (II) separation efficiency of the generated electron−hole pairs with electrons traveling toward the CdS side, and the holes toward the Cu$_2$S side; and (III) recombination rate between electrons and holes. For a certain PV device, the output voltage is nearly a constant, which depends on illumination intensity and temperature ($V_{OC}$ = $(E_{fn} − E_{fp})/q$), where $E_{fn}$ and $E_{fp}$ are the quasi-Fermi level of the electrons and holes under illumination, and $q$ is the electron charge, if the illumination intensity, working temperature, and the doping level of the p−n junction are fixed. In such case, the number of the light-generated electron−hole pairs is a constant. Thus, the performance of the PV device is mainly determined by the carrier separation, transport and recombination processes.

Since the p-Cu$_2$S shell is nonpiezoelectric and its size is only 10−15 nm, heavily doped, much thinner than the diameter of

the CdS core (up to tens of micrometers, such as 5.8 $\mu$m of the device in Figure 2d), our discussions mainly focus on the piezoelectric effect from the CdS core. With an assumption of low-doping in CdS for simplicity, numerically calculated piezopotential distribution in the CdS/Cu$_2$S core−shell NWs shows that a potential drop is created along its length when the CdS NW is under c-axis strain (Figure 5e,h). This is well proved by the numerous studies we have carried out for ZnO[27,28] and InN[29] nanogenerators and piezotronics.[30] For a PV device with configuration I, as shown in Figure 3 and Figure 5d, the local positive piezoelectric charges at the Cu$_2$S/CdS interface (Figure 5e) will lower the conduction and valence bands of CdS, as labeled in Figure 5f, resulting in a decrease of the barrier height at the hetrojunction interface. This is equivalent to an increase in the depletion width and internal field, which will accelerate the electron−hole pair separation process and reduce the possibility of recombination, thus enhancing the performance of the PV with the increase of the applied compressive strain. For a PV device with configuration II, as shown in Figure 4 and Figure 5g, the effect of the local negative piezopotential at the Cu$_2$S/CdS interface (Figure 5h) will lift up the conduction and valence bands of CdS, as labeled in Figure 5i, resulting in an increase of the barrier height at the hetrojunction interface. This is equivalent to a decrease in the depletion width and internal field, which will make the electron−hole pair more difficult to be separated and thus increase the possibility of recombination. Subsequently, the output current and the convention efficiency are decreased when the device is compressively strained. This is the basic mechanism of how does the piezo-phototronic effect tune the output efficiency of a solar cell.

In summary, we first demonstrated largely enhanced performance of n-CdS/p-Cu$_2$S coaxial NW PV devices using the piezo-phototronics effect when the PV device is subjected to an external strain. Piezo-phototronics effect could control the electron−hole pair generation, transport, separation and/or recombination, thus tuning the performance of the PV devices; when the p−n junction is parallel to the c axis of the NW (configure I), the PV performance enhances with increasing the compressive strain but decreases with increasing the tensile strain. This effect offers a new concept for improving solar energy conversation efficiency by designing the orientation of the nanowires and the strain to be purposely introduced in the packaging of the solar cells. This study shed light on the enhanced flexible solar cells for applications in self-powered technology, environmental monitoring, and even defensive technology.

## ASSOCIATED CONTENT

### Ⓢ Supporting Information
Additional information and figure. This material is available free of charge via the Internet at http://pubs.acs.org.

## AUTHOR INFORMATION

### Corresponding Author
*E-mail: zhong.wang@mse.gatech.edu.

### Notes
The authors declare no competing financial interest.

## ACKNOWLEDGMENTS

## REFERENCES

(1) Kempa, T. J.; Cahoon, J. F.; Kim, S. K.; Day, R. W.; Bell, D. C.; Park, H. G.; Lieber, C. M. Proc. Natl. Acad. Sci. U.S.A. 2012, 109 (5), 1407−1412.

(2) Tian, B. Z.; Zheng, X. L.; Kempa, T. J.; Fang, Y.; Yu, N. F.; Yu, G. H.; Huang, J. L.; Lieber, C. M. Nature 2007, 449 (7164), 885−U8.

(3) Tang, J. Y.; Huo, Z. Y.; Brittman, S.; Gao, H. W.; Yang, P. D. Nat. Nanotechnol. 2011, 6 (9), 568−572.

(4) Kayes, B. M.; Atwater, H. A.; Lewis, N. S. J. Appl. Phys. 2005, 97, 114302.

(5) Cao, L. Y.; Park, J. S.; Fan, P. Y.; Clemens, B.; Brongersma, M. L. Nano Lett. 2010, 10 (4), 1229−1233.

(6) Law, M.; Greene, L. E.; Johnson, J. C.; Saykally, R.; Yang, P. D. Nat. Mater. 2005, 4 (6), 455−459.

(7) Kim, D. R.; Lee, C. H.; Rao, P. M.; Cho, I. S.; Zheng, X. L. Nano Lett. 2011, 11 (7), 2704−2708.

(8) Pan, C. F.; Luo, Z. X.; Xu, C.; Luo, J.; Liang, R. R.; Zhu, G.; Wu, W. Z.; Guo, W. X.; Yan, X. X.; Xu, J.; Wang, Z. L.; Zhu, J. ACS Nano 2011, 5 (8), 6629−6636.

(9) Boxberg, F.; Sondergaard, N.; Xu, H. Q. Nano Lett. 2010, 10 (4), 1108−1112.

(10) Czaban, J. A.; Thompson, D. A.; LaPierre, R. R. Nano Lett. 2009, 9 (1), 148−154.

(11) Skold, N.; Karlsson, L. S.; Larsson, M. W.; Pistol, M. E.; Seifert, W.; Tragardh, J.; Samuelson, L. Nano Lett. 2005, 5 (10), 1943−1947.

(12) Hua, B.; Motohisa, J.; Kobayashi, Y.; Hara, S.; Fukui, T. Nano Lett. 2009, 9 (1), 112−116.

(13) Kim, D. H.; Lu, N. S.; Ma, R.; Kim, Y. S.; Kim, R. H.; Wang, S. D.; Wu, J.; Won, S. M.; Tao, H.; Islam, A.; Yu, K. J.; Kim, T. I.; Chowdhury, R.; Ying, M.; Xu, L. Z.; Li, M.; Chung, H. J.; Keum, H.; McCormick, M.; Liu, P.; Zhang, Y. W.; Omenetto, F. G.; Huang, Y. G.; Coleman, T.; Rogers, J. A. Science 2011, 333 (6044), 838−843.

(14) Rogers, J. A.; Huang, Y. G. Proc. Natl. Acad. Sci. U.S.A. 2009, 106 (27), 10875−10876.

(15) Yang, Q.; Guo, X.; Wang, W. H.; Zhang, Y.; Xu, S.; Lien, D. H.; Wang, Z. L. ACS Nano 2010, 4 (10), 6285−6291.

(16) Yang, Q.; Wang, W. H.; Xu, S.; Wang, Z. L. Nano Lett. 2011, 11 (9), 4012−4017.

(17) Shi, J.; Starr, M. B.; Xiang, H.; Hara, Y.; Anderson, M. A.; Seo, J. H.; Ma, Z. Q.; Wang, X. D. Nano Lett. 2011, 11 (12), 5587−5593.

(18) Gu, F. X.; Yang, Z. Y.; Yu, H. K.; Xu, J. Y.; Wang, P.; Tong, L. M.; Pan, A. L. J. Am. Chem. Soc. 2011, 133 (7), 2037−2039.

(19) Son, D. H.; Hughes, S. M.; Yin, Y. D.; Alivisatos, A. P. Science 2004, 306 (5698), 1009−1012.

(20) Robinson, R. D.; Sadtler, B.; Demchenko, D. O.; Erdonmez, C. K.; Wang, L. W.; Alivisatos, A. P. Science 2007, 317 (5836), 355−358.

(21) Luther, J. M.; Zheng, H. M.; Sadtler, B.; Alivisatos, A. P. J. Am. Chem. Soc. 2009, 131 (46), 16851−16857.

(22) Sadtler, B.; Demchenko, D. O.; Zheng, H.; Hughes, S. M.; Merkle, M. G.; Dahmen, U.; Wang, L. W.; Alivisatos, A. P. J. Am. Chem. Soc. 2009, 131 (14), 5285−5293.

(23) Jain, P. K.; Amirav, L.; Aloni, S.; Alivisatos, A. P. J. Am. Chem. Soc. 2010, 132 (29), 9997−9999.

(24) Bryant, F. J.; Glew, R. W. Energy Convers. 1975, 14 (3−4), 129−133.

(25) Yang, R. S.; Qin, Y.; Dai, L. M.; Wang, Z. L. Nat. Nanotechnol. 2009, 4 (1), 34−39.

(26) Tevelde, T. S. Solid-State Electron. 1973, 16 (12), 1305−1314.

(27) Gao, Y.; Wang, Z. L. Nano Lett. 2009, 9 (3), 1103−1110.

(28) Xu, S.; Qin, Y.; Xu, C.; Wei, Y. G.; Yang, R. S.; Wang, Z. L. Nat. Nanotechnol. 2010, 5 (5), 366−373.

(29) Huang, C. T.; Song, J. H.; Tsai, C. M.; Lee, W. F.; Lien, D. H.; Gao, Z. Y.; Hao, Y.; Chen, L. J.; Wang, Z. L. Adv. Mater. 2010, 22 (36), 4008−4013.

(30) Wang, Z. L. J. Phys. Chem. Lett. 2010, 1 (9), 1388−1393.